fibers

MDPI

Article

Experimental Investigation and Modelling of the Layered Concrete with Different Concentration of Short Fibers in the Layers

Vitalijs Lusis [1,*], Olga Kononova [1,2], Arturs Macanovskis [1,2], Rimvydas Stonys [3], Inga Lasenko [1] and Andrejs Krasnikovs [1]

[1] Department of Theoretical Mechanics and Strength of Material, Institute of Mechanics and Mechanical Engineering, Riga Technical University, 1 Kalku Street, LV-1658 Riga, Latvia; olga.kononova@rtu.lv (O.K.); arturs.macanovskis@rtu.lv (A.M.); inga.lasenko@rtu.lv (I.L.); andrejs.krasnikovs@rtu.lv (A.K.)
[2] Research Center for Ecological Construction, Riga Technical University, 1 Paula Valdena Street, LV-1048 Riga, Latvia
[3] Scientific Institute of Thermal Insulation, Vilnius Gediminas Technical University, Linkmenų g. 28, LT-08217 Vilnius, Lithuania; rimvydas.stonys@vgtu.lt
* Correspondence: vitalijs.lusis@rtu.lv

Abstract: The use of steel fiber reinforced concrete (SFRC) in structures with high physical-mechanical characteristics allows engineers to reduce the weight and costs of the structures, to simplify the technology of their production, to reduce or completely eliminate the manual labor needed for reinforcement, at the same time increasing reliability and durability. Commonly accepted technology is exploiting randomly distributed in the concrete volume fibers with random each fiber orientation. In structural members subjected to bending, major loads are bearing fibers located close to outer member surfaces. The majority of fibers are slightly loaded. The aim of the present research is to create an SFRC construction with non-homogeneously distributed fibers. We prepared layered SFRC prismatic specimens. Each layer had different amount of short fibers. Specimens were tested by four point bending till the rupture. Material fracture process was modelled based on the single fiber pull-out test results. Modelling results were compared with the experimental curves for beams. Predictions generated by the model were validated by 4PBT of 100 × 100 × 400 mm prisms. Investigation had shown higher load-bearing capacity of layered concrete plates comparing with plate having homogeneously distributed the same amount of fibers. This mechanism is strongly dependent on fiber concentration. A high amount of fibers is leading to new failure mechanisms—pull-out of FRC blocks and decrease of load-bearing capacity. Fracture surface analysis was realized for broken prisms with the goal to analyze fracture process and to improve accuracy of the elaborated model. The general conclusion with regard to modelling results is that the agreement with experimental data is good, numeric modelling results successfully align with the experimental data. Modelling has indicated the existence of additional failure processes besides simple fiber pull-out, which could be expected when fiber concentration exceeds the critical value.

Keywords: concretes; reinforced concrete; mechanical properties; steel fibers; single fiber pull-out; fibers distribution; modelling; numerical models

Citation: Lusis, V.; Kononova, O.; Macanovskis, A.; Stonys, R.; Lasenko, I.; Krasnikovs, A. Experimental Investigation and Modelling of the Layered Concrete with Different Concentration of Short Fibers in the Layers. *Fibers* **2021**, *9*, 76. https://doi.org/10.3390/fib9120076

Academic Editor: Giovanni Minafo

Received: 27 August 2021
Accepted: 22 November 2021
Published: 26 November 2021

1. Introduction

The field of building materials is immense and diverse. In the past decade, development and mass production of more efficient materials were among the main engineering challenges addressed in all industrial areas. Development of new, more efficient materials is an important task of the 21st century engineering. Nowadays, the building construction sector is the industrial area consuming the largest amount of materials. Concrete here is playing an important role. Despite long accumulated experience in using concrete,

its composition is being constantly improved and optimized, adjusting the mix for the purpose and objectives of specific applications [1]. A lot of research is done in this area, for example, in the field of lightweight fillers [2–4]. Impressive progress has been made in the construction industry since the introduction of the reinforced concrete. In most reinforced concrete constructions, concrete is strengthened with the bars made of different materials [5–11]. Plain concrete without additional reinforcement is frangible. Its tensile strength is low and short fibers, added as reinforcement, are able to improve the situation, simultaneously strengthening and toughening the material. In the modern construction, a concrete matrix is successfully reinforced with various fibers, applying various materials and methods [12–18]. Currently, fiber reinforced concrete (FRC) is increasingly used in various structural engineering applications.

The role of randomly distributed discontinuous fibers (homogeneous distribution) is to bridge the flanks of the crack, providing some post-cracking "ductility". If fibers are sufficiently strong and sufficiently bonded in the matrix material, the FRC may carry significant stresses over a relatively large strain region in the post-cracking stage (stage of visual crack formation and growing) [19–22]. It is believed that in the commercially used SFRC, fibers are evenly distributed in the concrete matrix volume. At the same time, homogeneous fiber distribution in the material volume is not necessary if a structural element made of SFRC is subjected, for example, to bending. Simultaneously, it should be taken into consideration that the material called "homogeneous" is not always homogeneous in reality, because during filling of the construction formwork (mix flowing process), fibers added to the concrete mix obtain non-homogeneous distribution and orientation in the fresh concrete volume, which inevitably affects the mechanical properties of FRC [23–28].

In the present research, layered SFRC with different amount of short fibers in plies were created, experimentally tested and analyzed. Numerical modelling was realized and modelling results were validated by experimental data. Plies internal geometry leading to increase of load-bearing capacity were recognized. Concentration of fibers in all specimens was 60 kg/m^3. In the specimens in Group A1, fibers were dispersed throughout the entire specimen volume, in the specimens in Groups A2–A8, fibers were distributed in layers with the specified fiber amount in each layer.

Increased local tensile strength compared with the concrete without fibers and the possibility to obtain "quasi"-plastic material behavior with a plateau in the stress-deformation curve are the main advantages of the steel fiber reinforced concrete (SFRC) in many engineering applications. A structural model may help gain better understanding of such processes as energy dissipation in the concrete matrix and fiber pull-out during cracking. In this research, such model is proposed for SFRC. Single fiber pull-out mechanics is used as the basis for the model, it is applied for description of experimental 4PBT results of the SFRC beams. The results of theoretical modelling were compared with the experimental data. Consideration of the bridging force of each fiber depending on the size of crack opening in the fiber location allows us to perform non-linear analysis of the breaking structure. The elaborated model can be used for development and analysis of other similar materials.

The issue of weight reduction of concrete structures has recently gained importance along with the growing demands towards construction materials saving, CO_2 reduction during cement production and further savings related to transportation. These concerns are not only economical but also environmental, since the concept of sustainable development is becoming more and more important.

2. Materials and Methods

Non-homogeneously layered SFRC prisms with dimensions of 100 × 100 × 400 mm were fabricated for the needs of the current investigation. The technology of specimen design is described in the invention patent of Riga Technical University [29]. Ten identical prisms of each type of non-homogeneous SFRC were cast.

2.1. Physical Properties of Steel Fibers

All SFRC specimens were made of the concrete containing commercially available hooked-ended steel fibers Bekaert, Dramix 3D RC 80/30BP. Fiber properties (supplier's data) are given in Table 1. Steel fiber geometry is shown in Figure 1. Aspect ratio is received dividing fiber length by its diameter.

Table 1. Specification of steel fibers according to supplier's data.

Fibre Type	Length, L_f, mm	Diameter, d_f, mm	Aspect Ratio, L_f/d_f	Density, kg/m^3	Modulus of Elasticity, GPa
Dramix 3D RC 80/30BP (Bekaert, Belgium)	30	0.38	79	7800	200

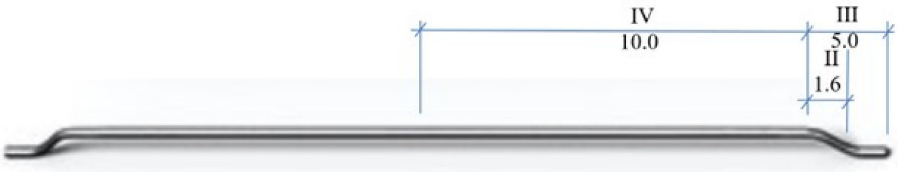

Figure 1. Geometry of steel fiber Dramix 3D RC 80/30BP (supplier's data).

Fibers are protected from corrosion in the alkaline environment of the cementitious matrix. Fibers do not have chemical bonds with the concrete, except for the acting Van der Waals forces, and their bond to the matrix can be enhanced by mechanical anchorage or surface roughness [30].

2.2. Concrete Mix Design and Materials

The concrete mix was designed using the tables and calculations provided in the standard EN-206. Concrete mix design: Portland cement, locally available crushed stone, sand (combination of 2 fractions and dolomite powder), pozzolanic admixture—silica fume, plasticizer and water, see Table 2.

Table 2. Concrete mix composition.

Composition	Weight, kg/m^3
Broken stone 4/8 mm (Saulkalne, Latvia)	900
Quartz Sand 0.3/2.5 mm (Saulkalne, Latvia)	620
Quartz Sand 0–1 mm (Saulkalne, Latvia)	120
Dolomite flour (Saulkalne, Latvia)	75
Portland cement CEM I 42.5N (SCHWENK Latvia Ltd., Latvia)	380
Silica Fume, grade 971U (Elkem, Norway)	25
Tap water, H_2O	170
Superplasticizer "Sikament 190" (Sika Baltic SIA, Latvia)	4
Fibers, steel 3D Dramix RC 80/30BP (Bekaert, Belgium)	60 (for all specimens A1–A8)

Samples for compression tests and determination of the concrete strength, as well as for the pull-out tests and 4PBTs, were prepared in accordance with LVS EN 12390-2: 2009, i.e., the formwork was removed after 48 h of curing at 20 ± 2 °C and 95% air humidity. The specimens were then cured by immersion in water at room temperature. Specimens were removed from water 24 h prior to testing, dried and tested at 28 days of age.

2.3. Preparation of Pull-Out Specimens

The pull-out tests on single steel fibers were performed using cured concrete specimens. A mould with two identical parts was used for each tested steel fiber. The size of one part is 50 × 50 × 30 mm (length × width × depth). A 0.5 mm thick separating film was places between the two parts of the mould, the moulds were oiled with the mould oil.

Figure 2 shows configuration of the pull-out test, where L/2—a half of the fiber length immersed in the matrix, α is fiber angle with regard to direction of the load applied in the pull-out test. For future numerical modelling (see this article chapter 4.4) α in experiments was equal to 90°. In order to prevent the fiber from being displaced when a concrete matrix is poured, the specimens (see Figure 3) were made according to the following procedure:

Step 1—one part of the mould was filled with concrete and after that L/2 of the fiber was immersed in the concrete oriented right to the vertical axis of the mould (direction of the pulling out force).

Step 2—after 24 h, the second part of the concrete matrix was filled and the oriented fiber did not change orientation, since the concrete in the first part of the matrix had hardened. The device shown in Figure 3 was used to cast 7 pull-out specimens simultaneously. One day later, the specimens were removed from the moulds and placed for hardening in the water bath at a constant temperature of 20 °C in accordance with LVS EN 12390-2: 2019.

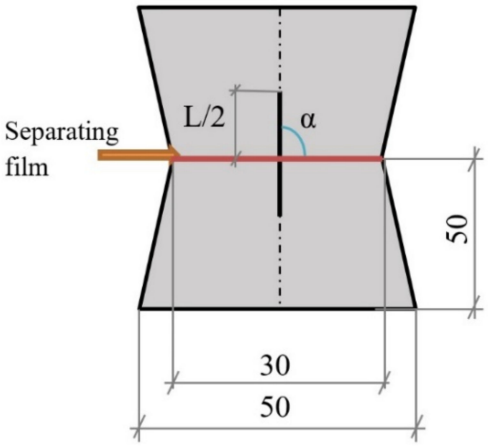

Figure 2. Single fiber pull-out test specimen scheme.

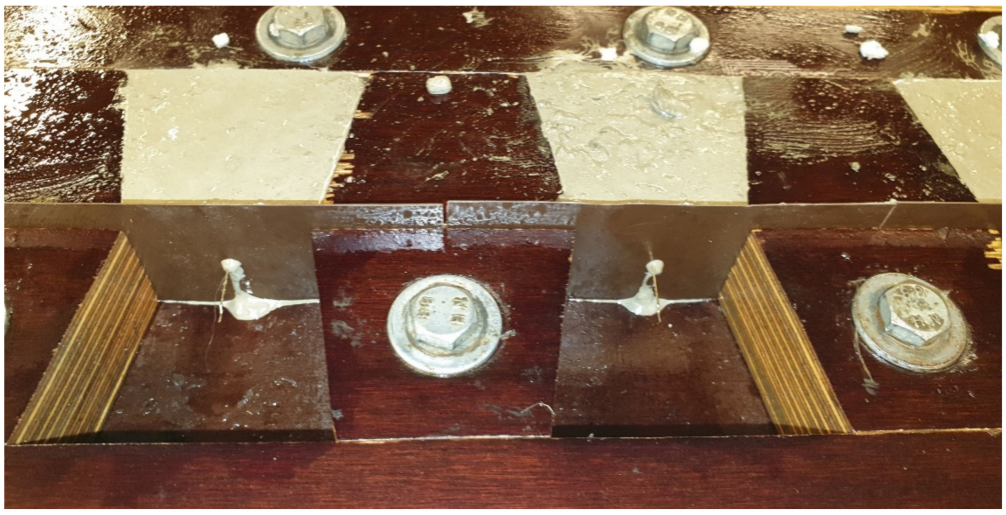

Figure 3. Step 1, preparation of pull-out samples.

2.4. Specimens' Preparation for Compressive Strength Testing and Curing Conditions

In order to carry out compression tests and determine the concrete strength, the specimens were prepared in the formwork with dimensions of 100 × 100 × 100 mm. The cubes were prepared according to similar concrete matrix mix design.

2.5. Specimen Preparation, Fiber Distribution and Concentration in the Layers of SFRC Prisms

Samples for 4PBT were prepared in the formworks with dimensions of 100 × 100 × 400 mm. Eight specimens of every type were cast with dimensions of 100 × 100 × 400 mm. Group A1—concrete samples with randomly (location and orientation) distributed fibers—consisted of SFRC with fibers added to the concrete at the stage of ingredients mixing–traditionally prepared SFRC. The formworks were filled with the SFRC, these prisms were used as a reference. It's worth mentioning—the total amount of fibers was the same in all eight groups of specimens. The difference between groups was in the fibers' distribution in the concrete volume. For specimens in Groups A2–A8, fibers were distributed in layers with various fiber concentrations and random 2D orientation. The height of each layer of SFRC reached 25 mm, while the length of the fibers was 30 mm.

A tool for fibers pressing consists of a set of steel disks. Discs were mounted on a shaft. Using discs as a "wheels" device was rolled over fibers along the formwork along the whole length of the prism according to the text of the RTU Latvian invention patent LV14257 [29]. Fiber distribution and concentration in the SFRC layers are given in Table 3. Specimens A2–A8 are essentially layered prisms.

Table 3. SF distribution and concentration in the SFRC layer kg/m^3.

Group No.	SF Concentration in Concrete Layers of the Specimen (From the Bottom up)
A1	100 mm × 100 mm—60 kg/m^3
A2	1 layer (from the bottom) 25 mm × 100 mm—120 kg/m^3 2 layer (from the bottom) 50 mm × 100 mm—concrete without SF 3 layer (from the bottom) 25 mm × 100 mm—120 kg/m^3
A3	1 layer (from the bottom) 30 mm × 100 mm—concrete without SF 2 layer (from the bottom) 25 mm × 100 mm—240 kg/m^3 3 layer (from the bottom) 45 mm × 100 mm—concrete without SF
A4	1 layer (from the bottom) 25 mm × 100 mm—160 kg/m^3 2 layer (from the bottom) 25 mm × 100 mm—80 kg/m^3 3 layer (from the bottom) 50 mm × 100 mm—concrete without SF
A5	1 layer (from the bottom) 25 mm × 100 mm—120 kg/m^3 2 layer (from the bottom) 25 mm × 100 mm—concrete without SF 3 layer (from the bottom) 25 mm × 100 mm—120 kg/m^3 4 layer (from the bottom) 25 mm × 100 mm—concrete without SF
A6	1 layer (from the bottom) 50 mm × 100 mm—120 kg/m^3 2 layer (from the bottom) 50 mm × 100 mm—concrete without SF
A7	1 layer (from the bottom) 25 mm × 100 mm—80 kg/m^3 2 layer (from the bottom) 25 mm × 100 mm—80 kg/m^3 3 layer (from the bottom) 25 mm × 100 mm—80 kg/m^3 4 layer (from the bottom) 25 mm × 100 mm—concrete without SF
A8	1 layer (from the bottom) 25 mm × 100 mm—240 kg/m^3 2 layer (from the bottom) 75 mm × 100 mm—concrete without SF

Following the specification, each group specimens were made filling the moulds by a concrete forming the current layer. On the top of the created ply was uniformly added necessary amount of fibers. Then fibers were gently pressed into the body of the last layer (see Figures 4–11).

Fibers were added to the concrete mix into the mixer and were mixed. Fibers obtained random distribution and orientation; at the same time, it was accepted that this distribution is uniform in volume and according to orientation. The specimen prepared using the classical method with fiber concentration of 60 kg/m^3 corresponds to group A1; it is shown in Figure 4.

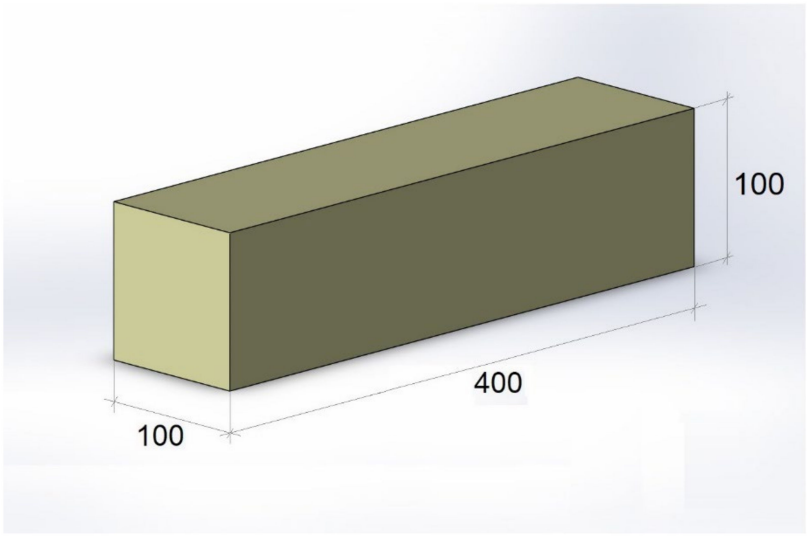

Figure 4. Sample with homogeneous fibers distribution in the volume (Group A1).

Group A2

1. The concrete layer, having thickness 25 mm, was created at the bottom of the formwork. One half of the total amount of fibers (60 kg/m^3) was evenly distributed on the upper surface of the layer and was stamped into the layer on whole its depth;
2. Second layer was 50 mm thick. Layer was without fibers;
3. Finally, the concrete layer 25 mm thick was added. It was SFRC layer with second half of the total amount of fibers (60 kg/m^3), see Figure 5.

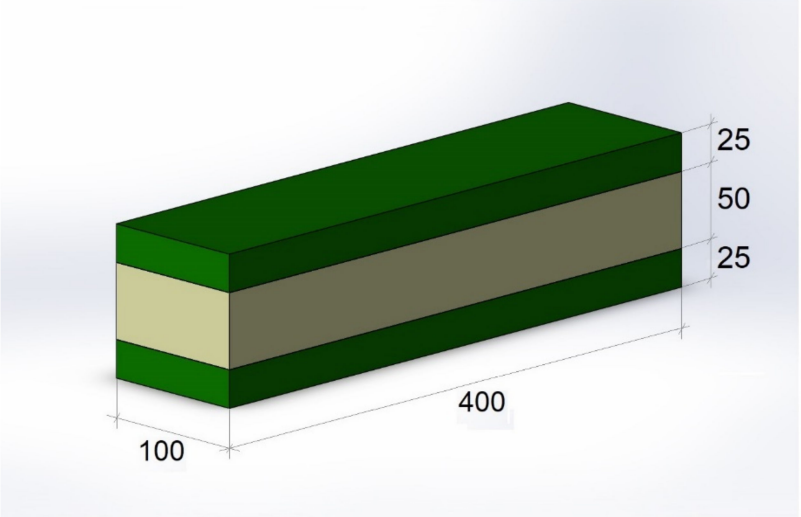

Figure 5. Fiber distribution in the prism of Group A2.

Group A3

1. 30 mm thick plain concrete ply was created at the bottom of the mold;
2. Then the layer with fibers, 25 mm thick, was added. The amount of fibers in the layer corresponded to total averaged over the prism volume fibers concentration equal to 60 kg/m^3;
3. Next layer—45 mm thick, was without fibers, see Figure 6.

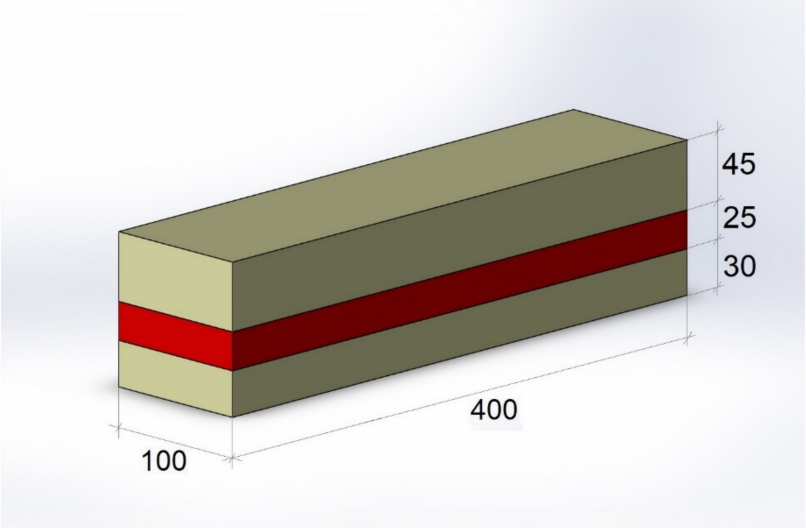

Figure 6. Fiber distribution in the prism of Group A3.

Group A4

1. The mould was filled with concrete to the height of 25 mm, then 2/3 of the total amount of fibers (60 kg/m^3) was uniformly distributed on the surface of the concrete in the formwork, then pressed and distributed in the concrete layer to the depth of 25 mm;
2. The mould was filled with the next concrete layer to the height of 25 mm and 1/3 of the total amount of fibers (60 kg/m^3) was pressed into the concrete filling to the whole depth of the concrete layer—25 mm;
3. 50 mm of concrete without fibers was added to the formwork, see Figure 7.

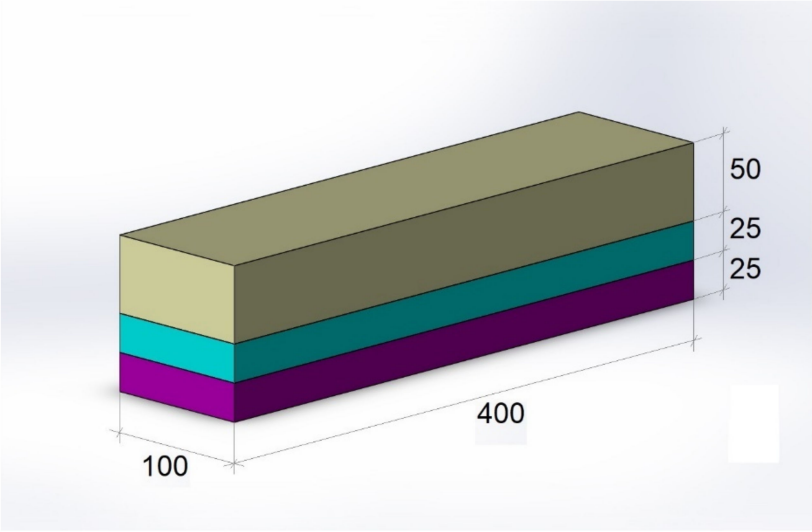

Figure 7. Fiber distribution in the prism of Group A4.

Group A5

1. The mould was filled with concrete to the height of 25 mm, then 1/2 of the total amount of fibers (60 kg/m^3) was uniformly distributed on the surface of the concrete in the formwork and pressed into concrete to the whole depth of the concrete layer of 25 mm;
2. 25 mm of the concrete without fibers were added into the formwork;
3. The next concrete layer of 25 mm was added and 1/2 of the total amount of fibers was distributed on its surface and pressed into the concrete to the whole depth of the concrete layer of 25 mm;
4. 25 mm of concrete without fibers was added to the formwork, see Figure 8.

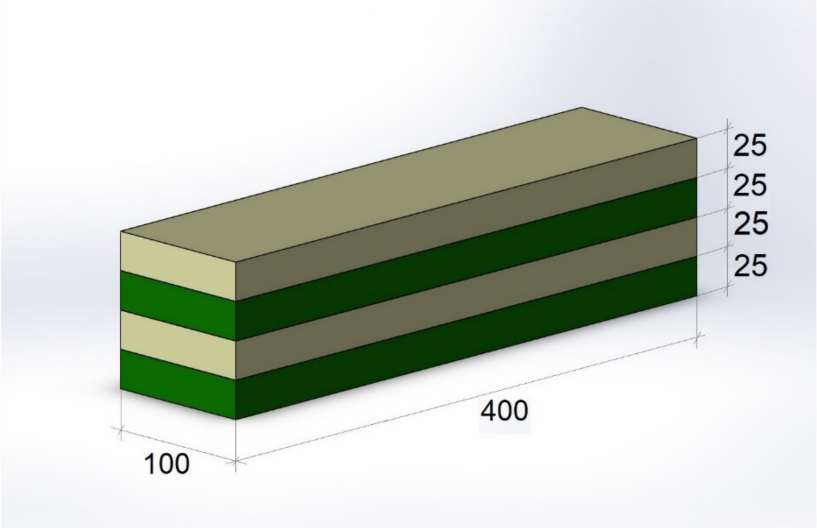

Figure 8. Fiber distribution in the prism of Group A5.

Group A6

1. The mould was filled with concrete to the height of 25 mm, then 1/2 of the total amount of fibers (60 kg/m^3) was uniformly distributed on the surface of the concrete in the formwork and pressed into the concrete to the whole depth of the concrete layer of 25 mm;
2. The mould was filled with concrete to the height of 50 mm, then 1/2 of the total amount of fibers was uniformly distributed on the surface of the concrete in the formwork and pressed into the concrete to the depth of the second concrete layer of 25 mm;
3. 50 mm of concrete without fibers was added to the formwork, see Figure 9.

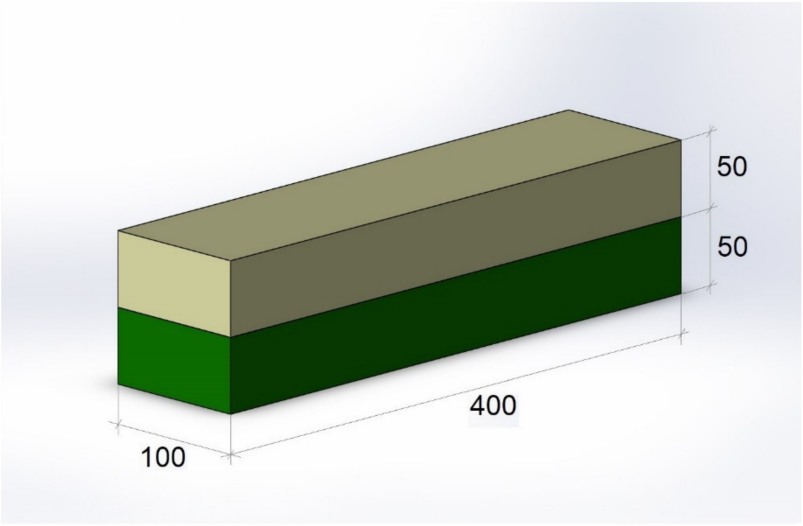

Figure 9. Fiber distribution in the prism of Group A6.

Group A7

1. The mould was filled with concrete to the height of 25 mm, then 1/3 of the total amount of fibers (60 kg/m^3) was uniformly distributed on the surface of the concrete in the formwork and pressed into concrete to the whole depth of the concrete layer of 25 mm;
2. The mould was filled with concrete to the height of 50 mm, then 1/3 of the total amount of fibers was distributed on the surface of the concrete in the formwork and pressed into the concrete to the depth of 25 mm of the last added concrete layer;

3. The mould was filled with concrete to the height of 75 mm, then 1/3 of the total amount of fibers was distributed on the surface of the concrete in the formwork and pressed into the concrete to the depth of 25 mm of the last added concrete layer;
4. 25 mm of concrete without fibers was added to the formwork, see Figure 10.

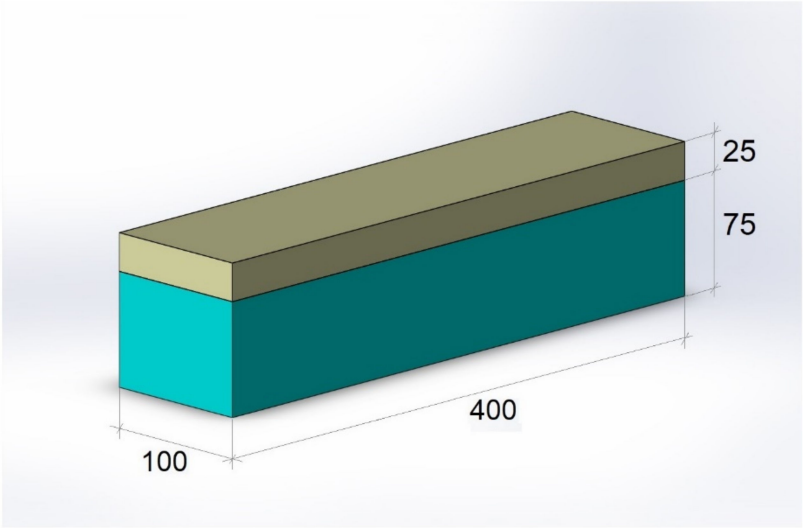

Figure 10. Fiber distribution in the prism of Group A7.

Group A8
1. The mould was filled with concrete to the height of 25 mm, then the total amount of fibers (60 kg/m^3) was uniformly distributed on the surface of the concrete in the formwork and pressed into concrete to the whole depth of the concrete layer of 25 mm;
2. 75 mm of concrete without fibers was added to the formwork, see Figure 11.

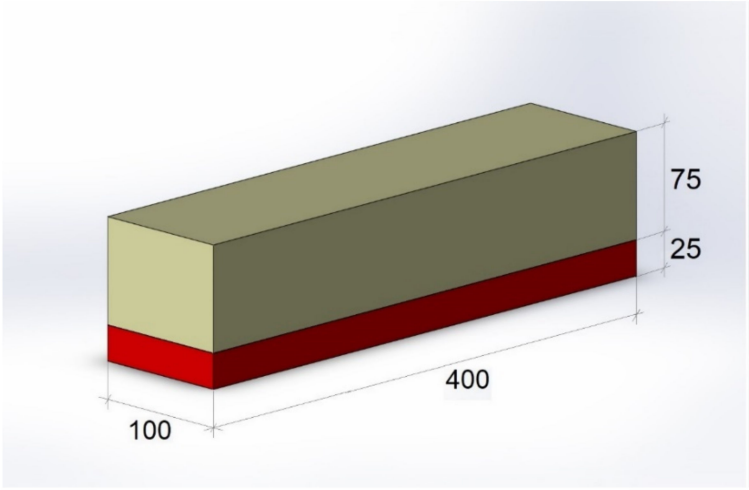

Figure 11. Fiber distribution in the prism of Group A8.

3. Mechanical Testing Methods

3.1. Description of Specimen Testing

After 28 days after their fabrication, the specimens were tested for fiber pull-out from the concrete matrix. Two parallel strips were glued on each concrete part of the specimen (Figure 12a) at an angle of 3 degrees and placed into testing machine grips. The video extensometer recorded the movement of the two glued strips (i.e., displacement of the steel fiber from the concrete matrix) (Figure 12b).

Test machine Zwick Roell Z150 (see Figure 12b) was used to determine the fiber pull-out force and the video extensometer Messphysik fixed the retractable fiber length. The pull-out was tested at the grip speed of 5 mm per minute.

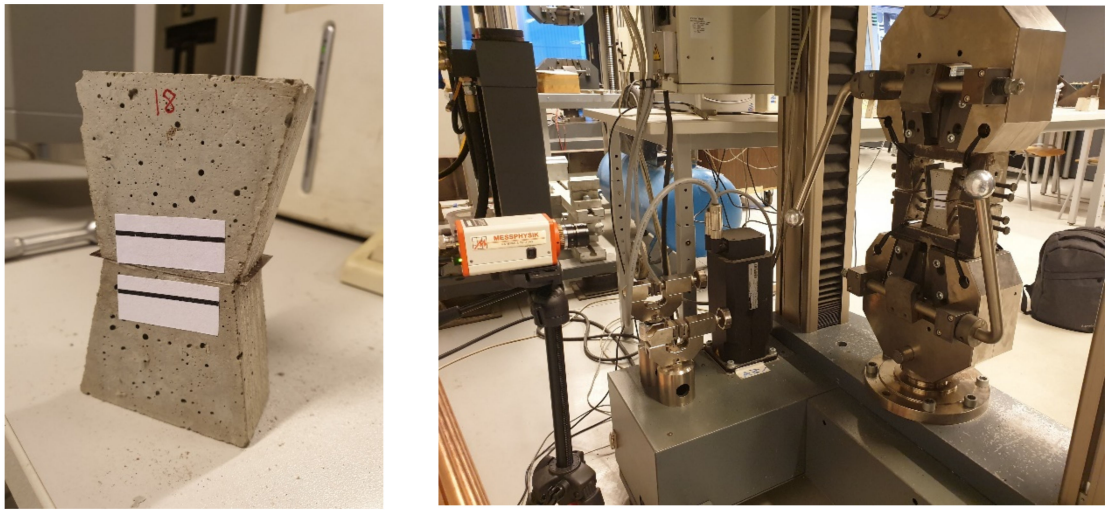

(**a**) (**b**)

Figure 12. (**a**) Pull-out sample; (**b**) Single steel fiber pull-out testing process.

3.2. Mechanical Testing. 4PBT Procedure

The setup scheme is shown in Figure 13. Verification of mechanical properties was carried out by 4PBT method using Controls Automax 5 loading machine. A frame with two HBM WA20 Linear Variable Displacement Transducers (LVDT) on its sides was used for recording the deformations in prisms during the tests.

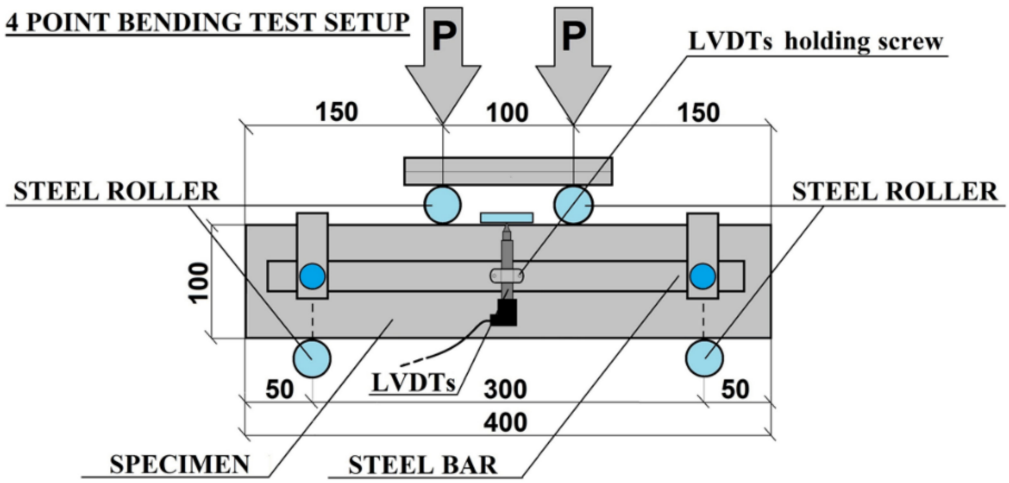

Figure 13. Four-point bending test scheme for testing of SFRC beams.

Load was applied in 0.25 kN steps for the period of 60 s. Deflection of the specimen was obtained by considering and summarizing the values from both sensors and obtaining the average value. The graphs visualizing the processes in SFRC, namely, behavior of the prisms with fibers under bending, were created. The load was applied until complete destruction of the specimens.

4. Experimental Results and Discussion

4.1. Fibers Pull-Out Process. Experimental Results

Figure 14 displays the process of pull-out of seven Dramix RC 80/30BP steel fibers from the concrete matrix and indicates the average values of the peak pull-out load. Four characteristic stages of the fiber pull-out process can be observed. At the first stage, at the load up of to 30 N, the fiber is getting deformed in the matrix without any pull-out. At the second stage, at the load of from 30 N to 150 N, the fiber starts to slide. Pulling out length is small (<1.6 mm); this is due to the fact that the fiber is bended at the ends—it has an anchor (the length of the anchor is 5 mm on each side of the fiber), which, being subjected to the bending stresses, resists when pulled out. At this stage, the greatest (maximum) load is obtained. When pull-out is up to ≈1.6 mm, the load reaches the average maximum value of 152.7 N. The distance 1.6 mm is the length at two bends of the anchor (see Figure 1). At the third stage, at the pull-out of from 1.6 mm to 5 mm, the fiber exhibits an intense decline in the applied pull-out force. When the length of the pulled-out fiber is up to 5 mm, the anchor part is pulled out of the matrix channel with friction. At these moments, the fiber is aligned (plastically deformed) [31–33]. At the fourth stage, the remaining fiber tail is pulled out. From 5 mm to 15 mm, the fiber is pulled out of the matrix channel with the decreasing force (Figure 14).

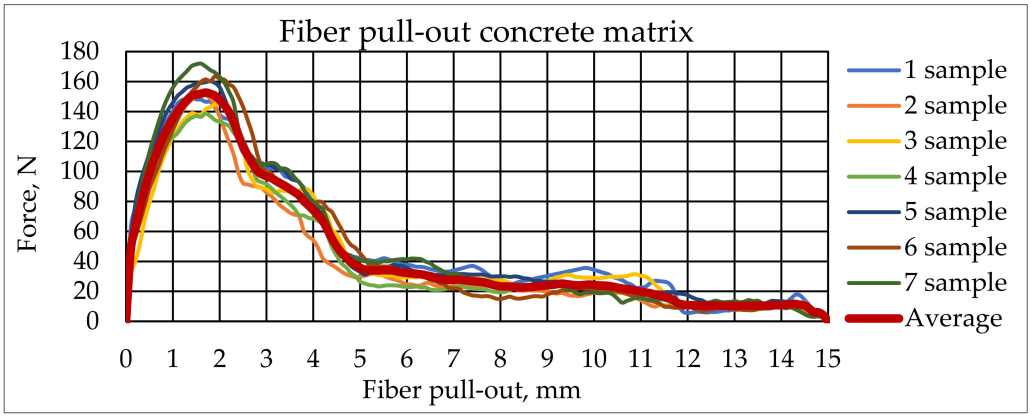

Figure 14. Fiber pull-out from the concrete matrix.

During the entire pull-out of the fibers, the jumps in the force value may be observed. This may be explained by the fact that spalling micro-particles of the concrete matrix are pulled with friction forming plugs [34,35]. We accepted that, fiber pull-out is the main crack opening mechanism that determines cracked prism load bearing at active cracking stage. In SFRC materials, SF and concrete matrix are bonded together through a weak interface. The study of this interfacial behavior is very important for understanding the mechanical behavior of SFRC. From a mechanical point of view, SF in FRC contribute to the increased tensile strength as well as prevent cracking and give certain quasi-plasticity to otherwise brittle concrete. By increasing the load, the crack opens and short SF carry the stresses over it. Due to the relatively weak bonding between concrete and surface of the SF (only Van der Waals bonds are formed), as well as due to the limited l/d ratio characteristic of almost all commercially available fibers, fiber rupture can be rarely observed. These results demonstrate that the pull-out response of the hooked fibers at the given embedded length is predominantly influenced by the mobilization and straightening of the hooks; the fibers are also pulled with friction, which is in accordance with the findings by published other authors. [36–38].

4.2. Testing Compressive Strength of the Specimens

Cubes of each specific type of concrete matrix were prepared. Material properties in compression test procedures for determination of the strength of a concrete cube can

be determined both by non-destructive methods [39–41] and by the classical destructive method in accordance with EN 12390-3. Standard compression tests of a cube in accordance with EN 12390-3 were carried out to determine the compressive strength of concrete using a Controls Automax 5 testing machine. Eight cube specimens were tested at the age of 28 days. It was determined that the compressive strength of concrete cubes without fibers corresponds to the concrete strength class C55/67 according to EN 206. The measured density of SFRC specimens was 2300 kg/m^3.

4.3. Mechanical 4PBT Results

Chaotically distributed fibers in the volume are used with the goal to resist micro-cracks formation, and their future propagation. In SFRCs having relatively not high fibers concentrations, main advantage is coming with adding fibers is realized after matrix cracking has occurred. Fibers crossing the crack are bridging its flanks, mitigating the crack opening process and growth. After the 4PB Test and based on their results, the average graphs were drawn. Average strength-deflection values were plotted using the MATLAB software. The graphs shown in Figures 15–22 illustrate the test results for the eight groups, respectively. Loading was until the macro-crack opening was reached 10–13 mm.

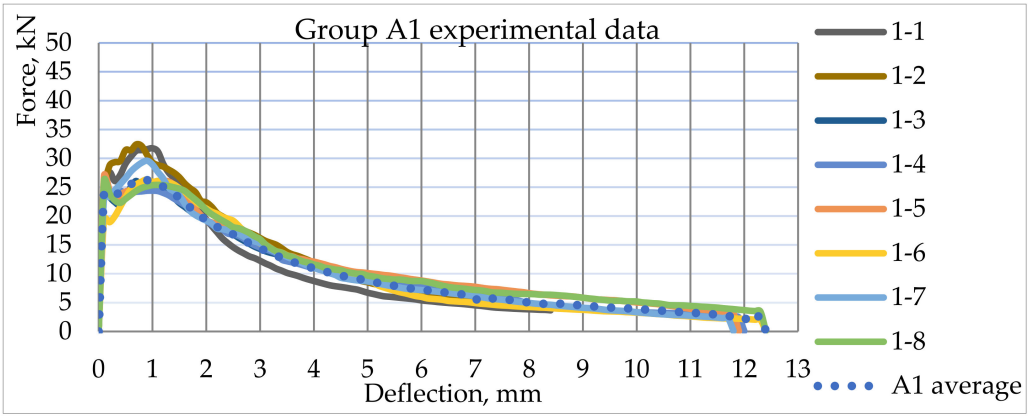

Figure 15. Load—sample center vertical deflection graphs for the specimens in the reference Group A1.

In the Figure 15 are shown experimentally obtained diagrams for specimens forming the Group A1. Along the vertical axis applied bending force is shown. Horizontal axis corresponds to each prism's central point vertical deflection value. Both the experimental curve of each specimen as well as the average value curve are shown. At each curve we can recognize three stages. First stage is linear elastic deflection (corresponds to deflection under 0.01 mm). At this stage, SFRC prisms become deformed without visible crack openings. Fibers in the concrete are not fully loaded and do not bear significant additional load. Second stage begins with the deviation of the curve from the straight line and terminates with reaching the maximum value on the curve (with middle point deflection of the prisms reaching 0.75 mm–1 mm).

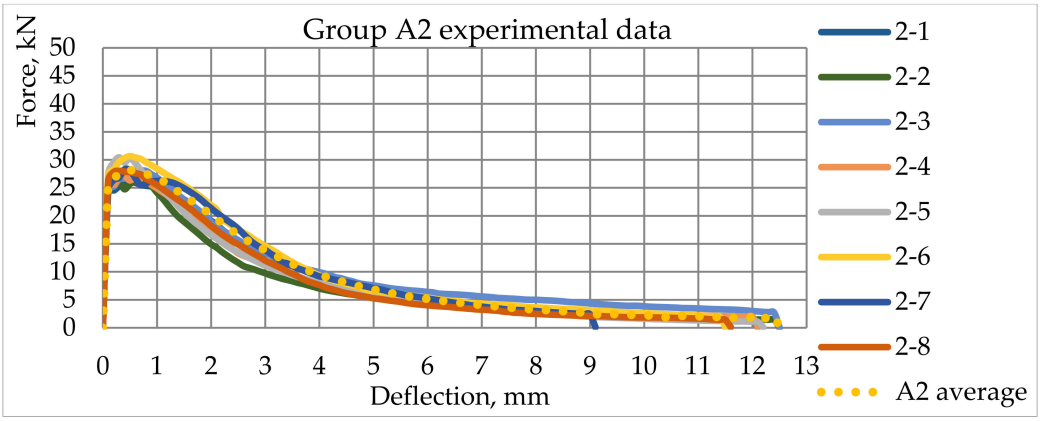

Figure 16. Load—sample center vertical deflection graphs for the specimens in Group A2.

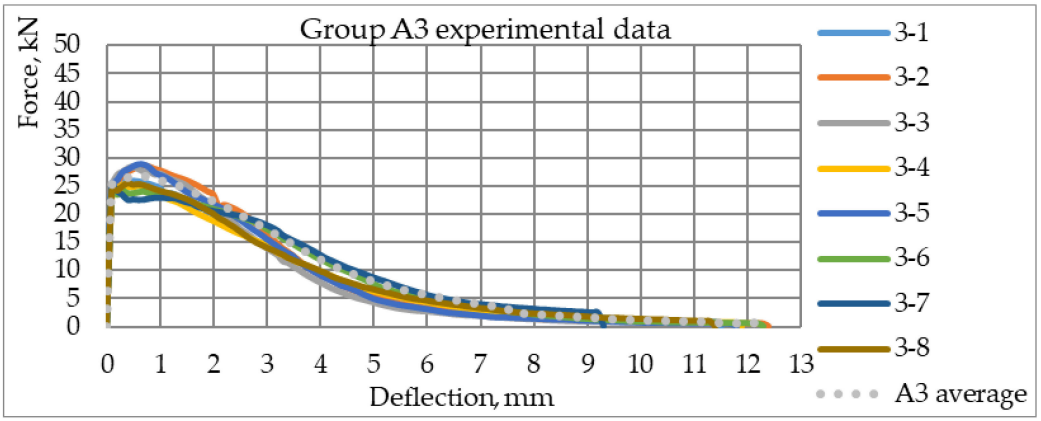

Figure 17. Load—sample center vertical deflection graphs for the specimens in Group A3.

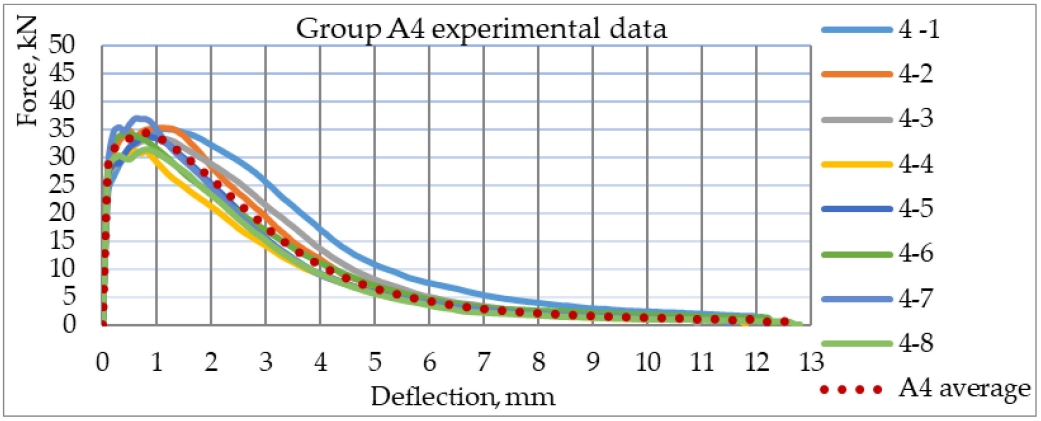

Figure 18. Load—sample center vertical deflection graphs for the specimens in Group A4.

At this stage, micro-cracks in the concrete grow and link, forming a macro-crack network. The macro-cracks are formed perpendicularly to the longitudinal axis of the prism (traditionally). Density of the macro-crack network depends on the specimen's geometry, size of the fibers, and their amount. The fibers crossing the macro-cracks begin to bear load, while cracks are still invisible on the outer surface of the specimen.

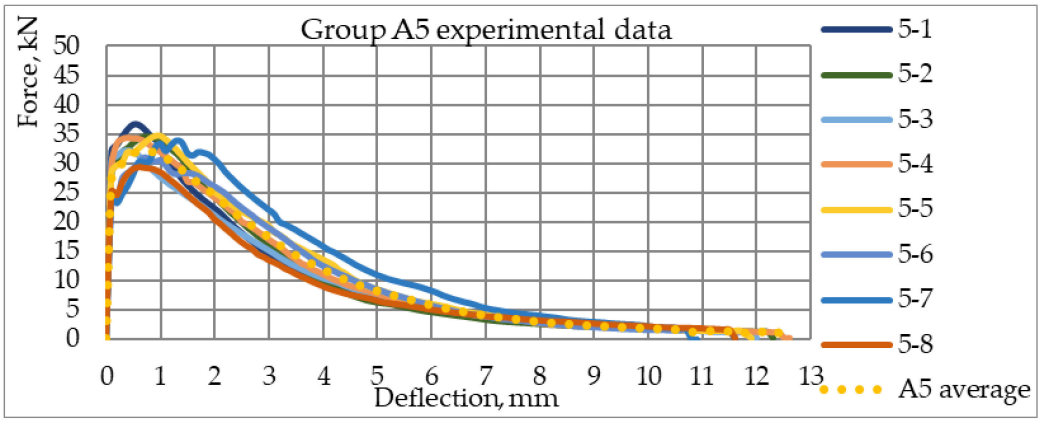

Figure 19. Load—sample center vertical deflection graphs for the specimens in Group A5.

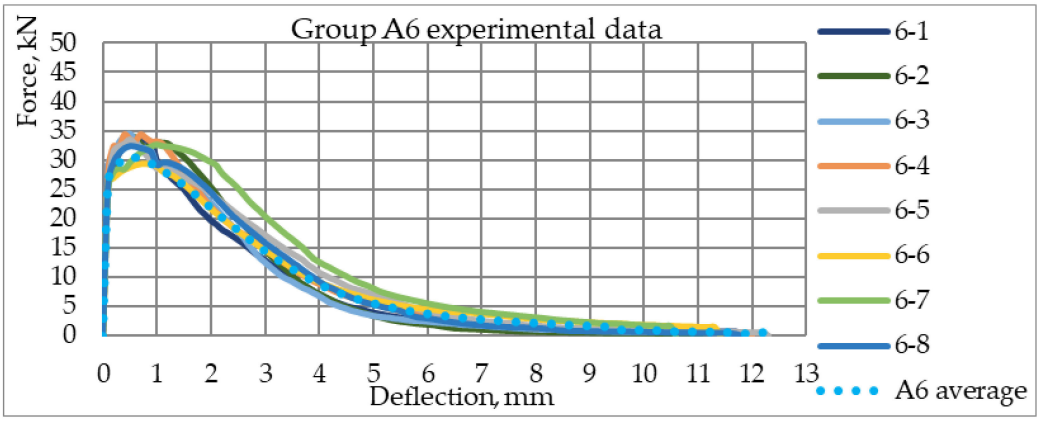

Figure 20. Load—sample center vertical deflection graphs for the specimens in Group A6.

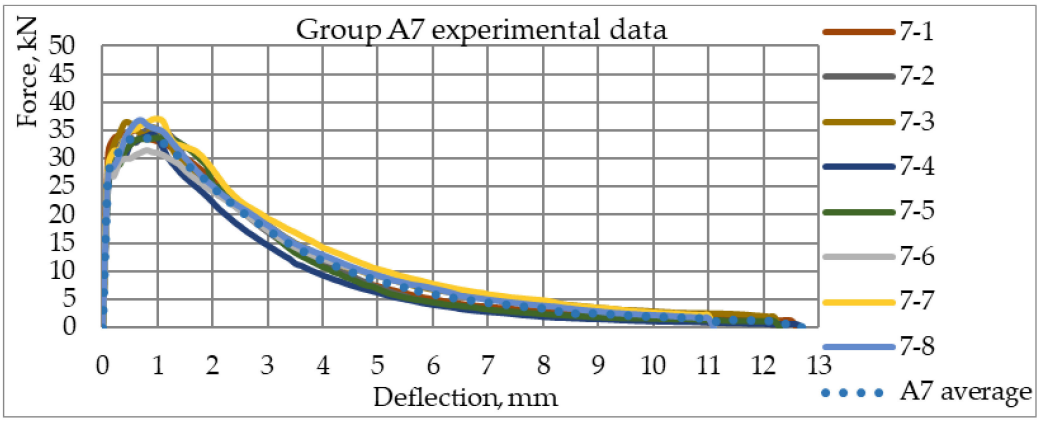

Figure 21. Load—sample center vertical deflection graphs for the specimens in Group A7.

The cracks with the lowest load carrying capacity, the ones with the lowest amount of fibers crossing the macro-crack, or the crack with the crossing fibers located and oriented in a less optimal way, start to open. They proceed in the following way: fibers bearing the load detach from the concrete and start pulling out from one or both sides. Individual load carrying capacity of a single fiber depends on its orientation towards the crack plane and how far it is extracted.

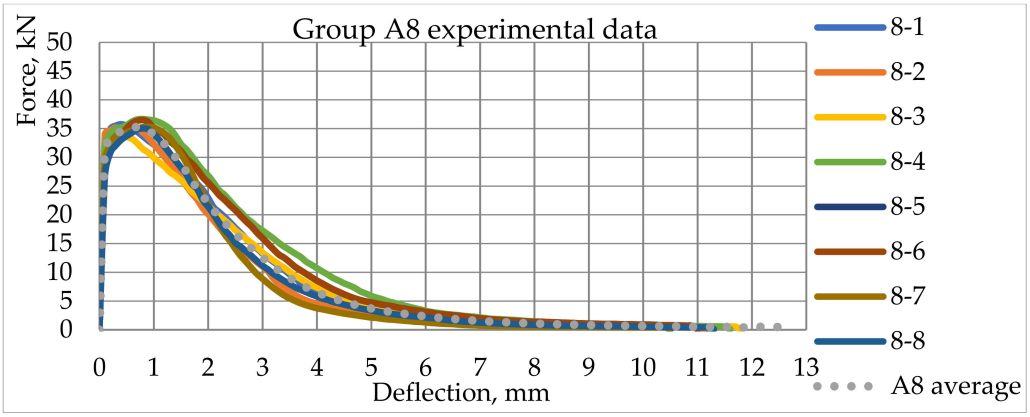

Figure 22. Load—sample center vertical deflection graphs for the specimens in Group A8.

Experimental observation of the micromechanics of fiber pull-out showed that the maximum load carrying capacity of a single fiber depends on its orientation towards direction of pulling out force and how much the fiber has been pulled out. Another factor is fiber declination angle to the direction of the pull-out force. Observations showed that the current value of the pull-out force decreases proportionally to the size of the crack opening; all these factors are confirmed, for example, by the following studies [42–44].

Experimental average curves for all eight groups are given in Figure 23. As it can be observed, Group A8 reaches the highest load carrying capacity during the initial stage of crack opening (crack opening 0–3.5 mm) due to the highest concentration of fibers compared to other groups in the lower part of the prism, which bears the maximum tensile load (see Figure 24). Similar situation can be observed performing numerical simulations, see Figures 25–32. As it can be concluded analyzing the obtained graphs, Group A1 (reference specimens) reaches lower average load carrying capacity compared to the specimens with non-homogeneous distribution of fibers. Similar tendencies can be observed studying the diagrams of average results of the specimens—the maximal load carrying capacity is reached with deflection of prisms 0.75 mm–1 mm, which correlates with the crack opening size.

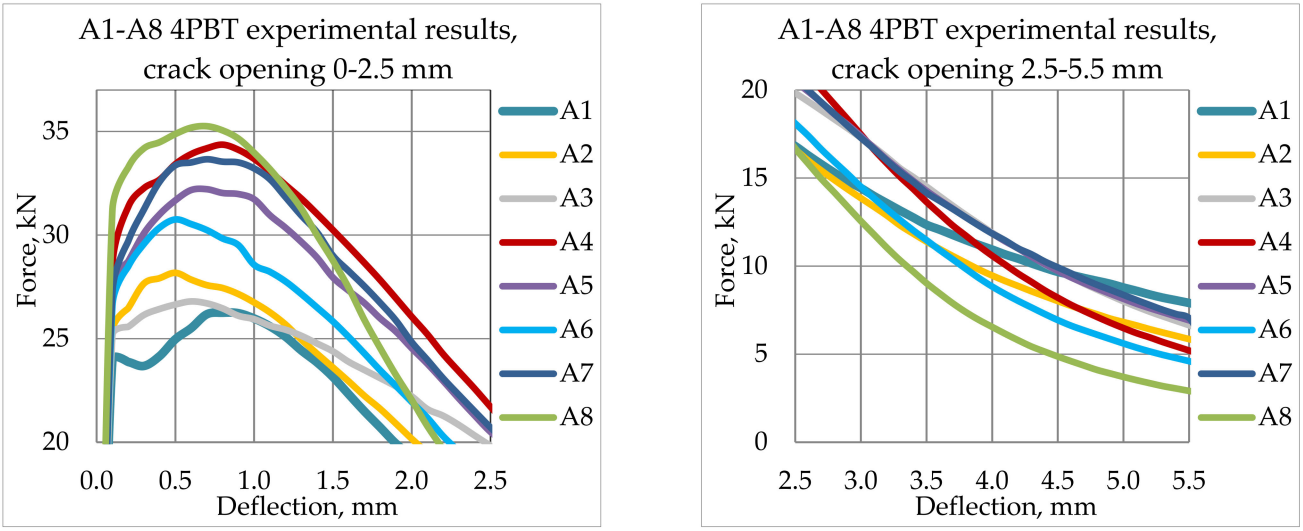

Figure 23. Average 4PBT experimental result curves of all specimen groups.

The situation changes at the stage when the crack opens to 2.5–5.5 mm. High local concentration of fibers in a relatively thin layer leads to additional cracking in this area

and immediate decrease of the load bearing capacity (samples in Group 8 carry lower load compared with Group 1).

After analysis of the results and the obtained information it can be stated with certainty that using the latest SFRC technologies—dividing fibers in certain layers—it is possible to reach the desired effect; in other words, fiber distribution has a significant impact on the tensile strength of the SFRC. Also, after laboratory experiments with non-homogenous SFRC including testing of the specimens as well as analysis and comparison of the results, considering that equal amount of SF was used in 1 m^3 of the concrete mix, the prisms with non-homogeneous fiber distribution, which demonstrate the highest load bearing capacity, were received by distribution of fibers.

It can be seen that SF can increase the bending resistance of the concrete structural element, when SF are distributed optimally.

The following conclusions can be drawn based on the results of this research. The presence and distribution of SF significantly improve the post-peak behavior, namely, the flexural tensile strength of the SFRC.

The adopted technological method of fiber distribution reached higher values of flexural strength for the SFRC comparing with homogenous fiber distribution in the volume of the beam according to the results of the flexural testing of the layered specimens. Non-homogenous fiber distribution also shows a positive effect, which differs from the result that could be expected—at the identical values of the flexural strength, the consumption of fibers will be lower for the SFRC with non-homogenous fiber distribution. Using this technology, it is possible to build SFRC structures with improved structure and better physical and mechanical properties.

Bending structures have highly heterogeneous stress fields ranging from the maximum tensile stress in the tensile zone to the maximum compression stress in the compression zone and being zero near the neutral axis, see Figure 24. For most of the statically loaded reinforced concrete structures trajectories of the main tensile stresses are easily determinable and known in advance. It is useful to incorporate SF in the tensile zone of the structure with the maximum tensile stresses. Therefore, with the same amount of fibers in homogenous and non-homogenous SFRC, it is possible to obtain better flexural strength results of the building element.

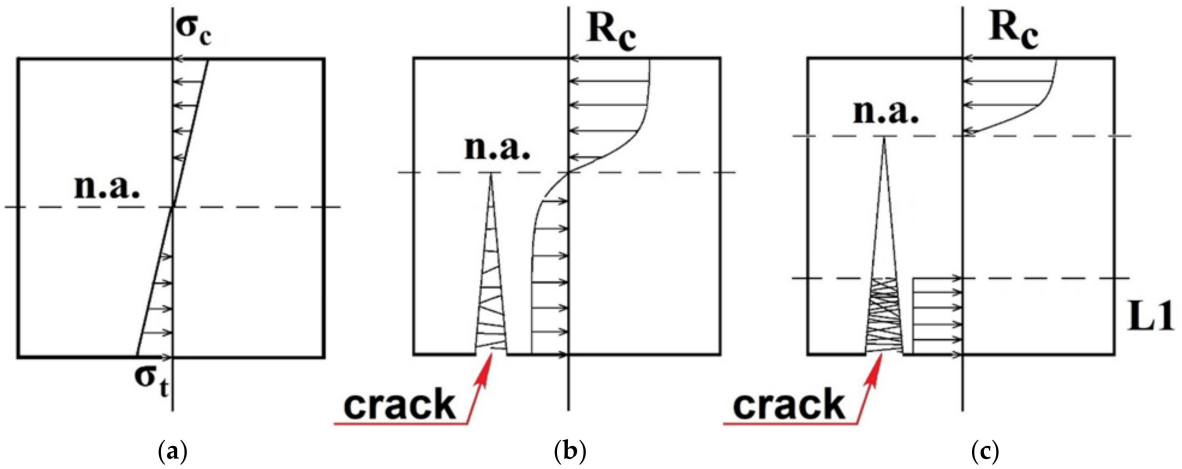

Figure 24. Distribution of stresses in the bended SFRC beam: (**a**) without crack; (**b**) with a macro-crack in the concrete with homogeneously distributed fibers (Group 1); (**c**) with a macro-crack and one layer with fibers (Group 8).

Significantly higher flexural strength of the non-homogenous SFRC was confirmed with the results of the bending test of the respective specimens, see Figure 23.

4.4. Numerical Modelling of SFRC Cracking Process

In the course of research, a model suitable for estimating the load-bearing capacity of bended SFRC structures with non-homogeneous fiber distribution in them has been developed. It is based on the observation that the load-bearing capacity of FRC elements is directly linked to the fiber pull-out resistance.

Computer modelling was performed using a numerical model *MATLAB*. The structural model of the opening of the macro-cracks in the prisms was developed using the previous modelling experience [45,46] and the results of testing of the micromechanics of the fiber pulling obtained in this study. The mechanical behavior of SFRC depends on the amount, orientation and the spatial distribution of the fibers, and geometry of the particular fiber, as well as design of the concrete matrix mix and the way concrete mix is placed into the formwork [47–52]. Fiber concentrations in the specimens and every particular layer of the specimen are given in Table 3.

FRC failure in 4PBT was simulated using a simple statistical model based on the average pull-out curve for a given fiber. After receiving the pull-out, the curve was appropriately processed. The fact is that during the experiment, at the initial stage, the so-called "play in the grips" occurred—when pulling the fiber from the concrete matrix, the fiber gradually selected the gaps available in the fiber—matrix-grips system. Thus, the initial pull-out curve was trimmed and shifted relative to the abscissa axis, and a portion of the pull-out curve with a pronounced nonlinearity was used for modelling, as shown in Figure 25. This kind of "trimming" allows for correct localization of the peak of the 4PBT fracture curve.

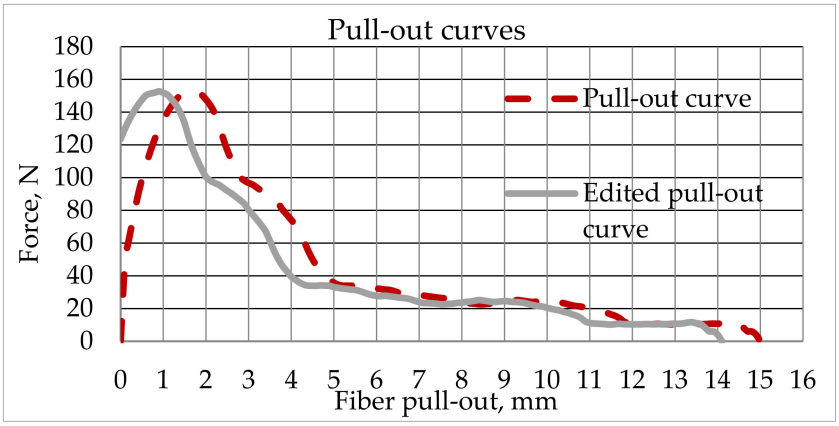

Figure 25. Real and edited pull-out curves.

During the modeling, a number of assumptions were made, and one of them is that fibers in the fiber-reinforced concrete are evenly distributed. First of all, the amount of fiber in the concrete matrix was determined. The number of kilograms of fiber per 1 m^3 was specified. Knowing the density of the fiber material, the diameter and the reduced (straightened) length of the fiber, the amount of fiber in 1 m^3 of concrete was determined, and then calculated proportionally for a concrete prism with dimension 100 × 100 × 400 mm.

Next, it was determined how many centers of gravity of the fibers were located in the elementary volume—the coefficient of fiber concentration k: e = 1 mm (along the length of the sample) × h = 5 mm (along the height of the sample) × 100 mm (along the depth of the sample), as shown in Figure 26. The resulting coefficient k was multiplied by an additional coefficient 2/3, since not all fibers in the sample were located strictly horizontally and perpendicular to the crack surface.

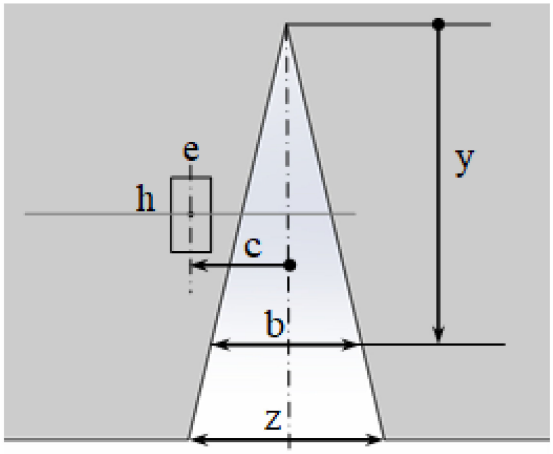

Figure 26. Crack geometry.

The results were processed in 3 nested loops.

The outer loop—by z dimension—represented mouth opening displacement. Changes from zero with the step of 0.1 mm to the maximum mouth opening displacement were fixed during the experiment until the sample was completely destroyed.

The middle loop—along c dimension—represented the distance from the fiber center of gravity to the crack plane. The middle loop makes it possible to consider in the calculation not only the fibers that lie directly in the plane of the crack, but also the fibers, whose centers of gravity are at a certain distance. c changes with step e = 0.5 mm to L/2-e, where L is the fiber length.

The inner loop—along y dimension—is the crack height, y varies from 0 to 0.8 H, where H is the sample height, with a step h = 0.5 mm, where h is the height of the elementary volume. As a result of experimental studies, it was found that the crack height at 4-point bending of a concrete sample was usually 0.8 of the total sample heights. The value of b was calculated inside the inner loop, that is, a full iteration of all variables z, c, and y was performed. b value was calculated using the Formula (1):

$$b = y \times z/0.8 \times H, \quad (1)$$

For each value b, the corresponding value P_{po} (force from pull-out curve) was selected from the pull-out curve. The bending moment in the crack M was determined by the Formula (2):

$$M = 2 \times k \times P_{po} (y - 0.5 \times h), \quad (2)$$

Thus, the bending moment M depends on the fiber concentration coefficient k and the fiber localization in the crack. Coefficient 2 was used because in the previous calculation only one crack edge was considered. Further, the bending moment was recalculated into force P, which was applied in 4PBT of the sample, see Formula (3):

$$P = 2 \times M/100, \quad (3)$$

4.5. SFRC Prisms Numerical Modelling Results

A model suitable for estimating the load-bearing capacity of the SFRC beam subjected to bending was developed.

Load bearing—vertical deflection at the center of the prisms of the specimens of Groups A1–A8 are shown in Figures 27–34. Experimentally obtained averaged curves were validated by the results of the numerical simulation for the prisms with fibers distributed in the cross-section of each prism according to the rules mentioned in Table 3.

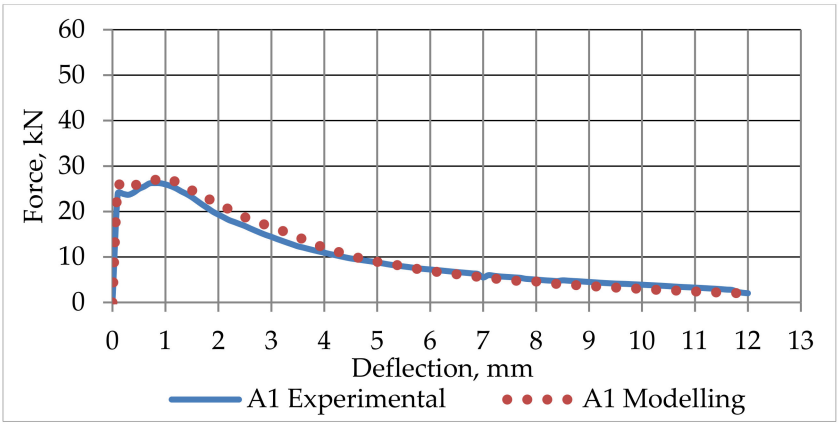

Figure 27. Experimental and modelling graphs for Group A1.

The modelling results are quite well approximating by the experimental data at first, second and third loading stages for samples in groups A1, A2, A5 and A7. Bad approximation at second stage is for specimens in groups A4, A6, A8. Judging from modelling results presented in Figures 30, 32 and 34, the agreement with experimental data depends on the fiber fraction in the mix.

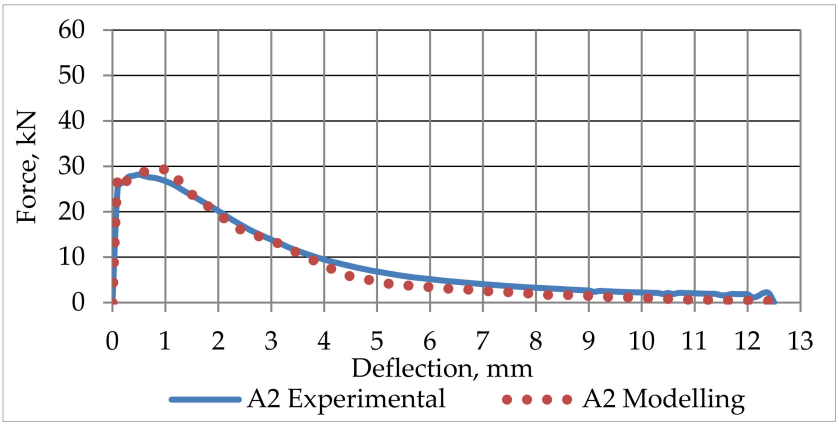

Figure 28. Experimental and modelling graphs for Group A2.

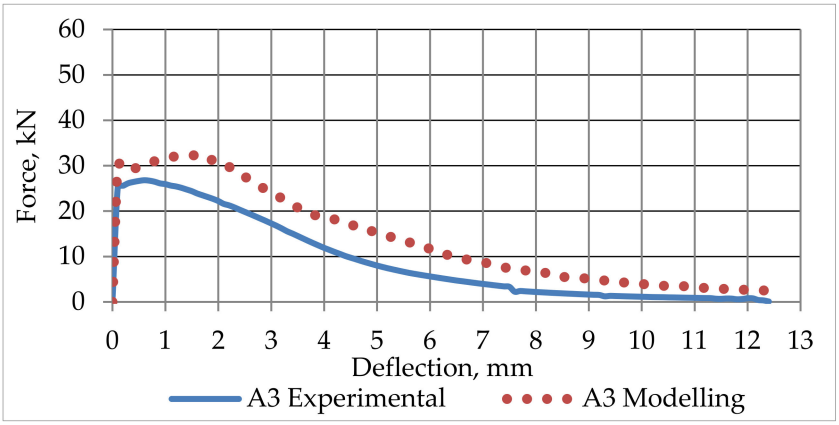

Figure 29. Experimental and modelling graphs for Group A3.

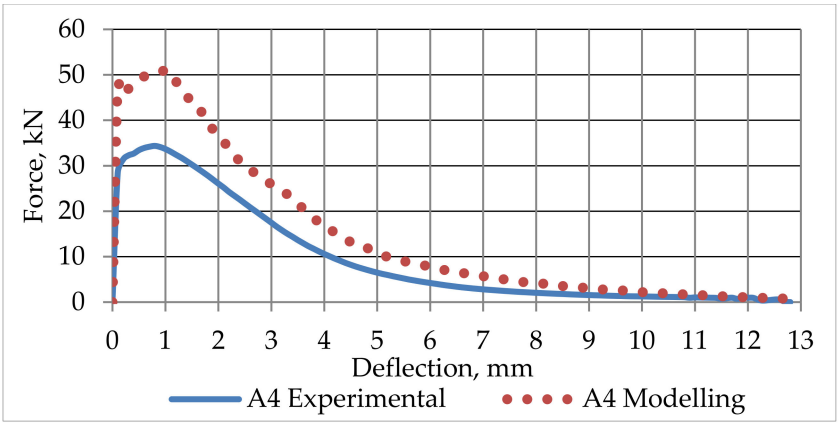

Figure 30. Experimental and modelling graphs for Group A4.

High local concentration of fibers in relatively thin layer leads to additional cracking in this area and, as was mentioned earlier, immediate decrease of the load bearing capacity (not included in the model). A possible reason for the deviation from the experimental data could also be that fiber orientation in the layers is contrary to modelling assumptions about random distribution across the volume and random distribution of orientation angles.

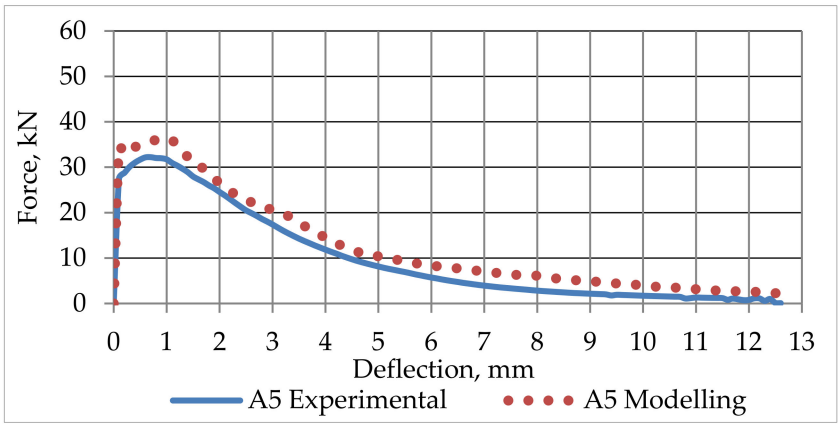

Figure 31. Experimental and modelling graphs for Group A5.

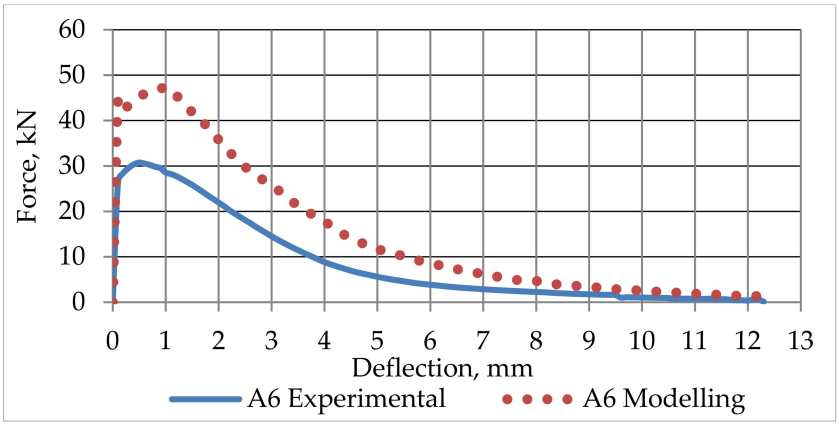

Figure 32. Experimental and modelling graphs for Group A6.

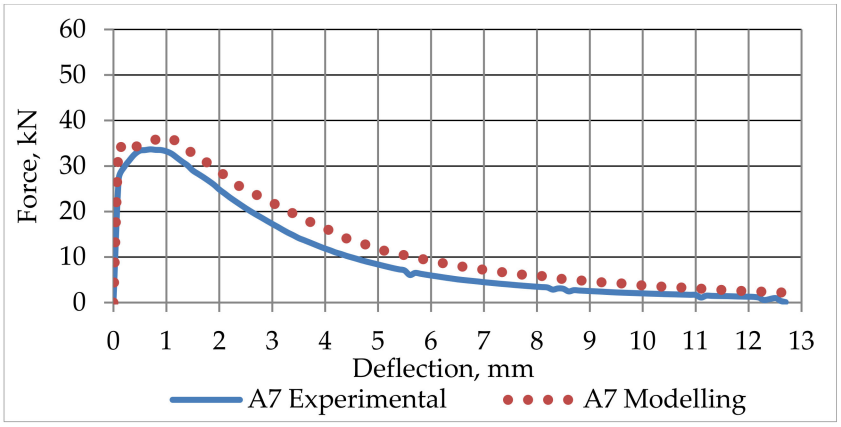

Figure 33. Experimental and modelling graphs for Group A7.

At the third stage, modelling results show higher load carrying capacity for the specimens compared to the ones obtained experimentally. The difference grows proportionally to the size of crack opening. It can be explained by the homogenous distribution of the fibers in the model in contrast to non-homogenous distribution in reality. Specimens in Group A8 in the experiment and simulation showed the best result, because the concentration of fibers in the bottom part of the prism was four times higher compared with the reference prism in Groups A1.

It can be concluded that the modelling results are consistent with the experimental data with regard to the pull-out power and displacement relation. Some critical concentration of fibers exists, dependent on the fiber type, length, concrete strength, and granulometry. When this concentration is exceeded, fibers start to "communicate" among themselves in the cracking processes, which leads to rapid decrease of the load-bearing capacity. The created model can be used practically in the numeric model for estimating the load-bearing capacity in the cracking and predicting the crack opening stage of the homogenous SFRC elements and SFRC elements with fiber distribution. Also, it has been proven that the numeric modelling accurately describes the load-bearing capacity of non-homogenous SFRC in the cracking stage.

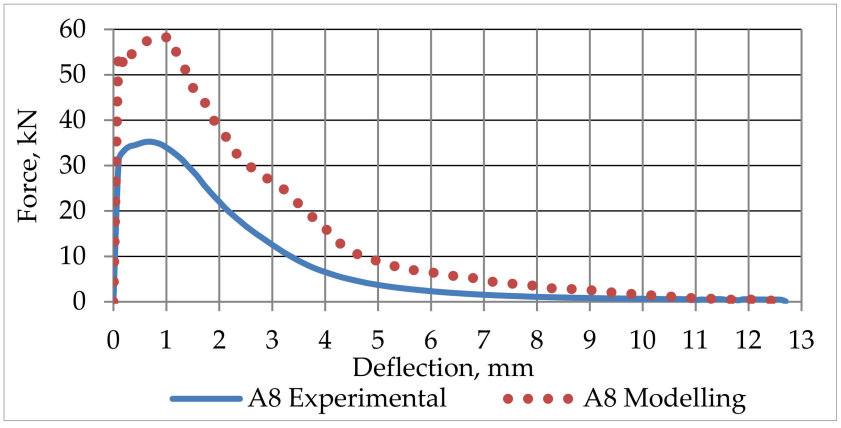

Figure 34. Experimental and modelling graphs for Group A8.

5. Conclusions

This study is presenting performed analysis of different types of fiber-concrete beams with layered fiber distribution in the concrete beam volume. The following conclusions were drawn from the obtained results.

According to the experimental testing results, the specimens in Group A8, A4, and A7 reached the highest load carrying capacity during crack opening stage, as they had

the highest concentration of fibers in the section of the prisms experiencing the maximum tensile load. The specimens in Group A1 showed lower average load carrying capacity during crack forming stage compared to the specimens with non-homogeneous fiber distribution. Fiber reinforcement can significantly increase the bending and shear resistance of concrete structural element, when steel fibers are working optimally. Specimens showed typical tri-linear variation in their load-deflection, load-crack mouth opening and load-crack tip opening displacement curves under flexure. There is some critical concentration of fibers dependent on the fiber type, length, concrete strength and granulometry, exceeding which the fibers start to "communicate" in the cracking processes, leading to the rapid decrease of load-bearing capacity.

Detailed numerical model has been elaborated. Modelling results allowed recognize the change of the failure mechanism along with the fiber content increase in the SFRC layers.

The general conclusion with regard to modelling results is that the agreement with experimental data is good; numeric modelling results successfully align with the experimental data. Modelling has indicated the existence of additional failure processes besides simple fiber pull-out, which could be expected when fiber concentration exceeds the critical value.

The validated method for creating non-homogeneous FRC consists in the metered incorporation of fibers into any layer of the construction. This technology allows changing fundamentally the use of SFRC, since it is possible either to reduce fiber consumption in general or to ensure higher load-bearing capacity of constructions, to reduce construction volume, weight, and building expenses at the usual volume of fiber consumption.

Author Contributions: Conceptualization, V.L. and O.K.; methodology, V.L., O.K., R.S. and I.L.; validation, V.L., O.K., R.S., I.L. and A.K.; formal analysis, V.L., O.K., R.S., I.L. and A.K.; investigation, V.L., A.M. and I.L.; resources, V.L., R.S. and A.K.; original draft preparation, V.L., O.K. and A.M.; review and editing, V.L., O.K. and A.K.; supervision, V.L., O.K. and A.K.; funding acquisition, V.L. All authors have read and agreed to the published version of the manuscript.

Funding: This work has been supported by the European Regional Development Fund within the Activity 1.1.1.2 "Post-doctoral Research Aid" Grant No.1.1.1.2/VIAA/2/18/324.

Institutional Review Board Statement: Not applicable.

Informed Consent Statement: Not applicable.

Data Availability Statement: All data are in the paper.

Acknowledgments: The authors would like to thank The State Education Development Agency (VIAA) Republic of Latvia for financial support in the framework of the European Regional Development Fund within the Activity 1.1.1.2 "Post-doctoral Research Aid" of the Specific Aid Objective 1.1.1 "To increase the research and innovative capacity of scientific institutions of Latvia and the ability to attract external financing, investing in human resources and infrastructure" of the Operational Programme "Growth and Employment" (Grant No.1.1.1.2/VIAA/2/18/324).

Conflicts of Interest: The authors declare no conflict of interest.

References

1. Sahmenko, G.; Rucevskis, S.; Lusis, V. The study of the combined effect of fly ash, silica fume, colloidal silica and superplasticizer on high performance cement composite applying mix optimization method. *Mech. Compos. Mater.* Unpublished manuscript.
2. Adesina, A. Sustainable application of cenospheres in cementitious materials—Overview of performance. *Dev. Built Environ.* **2020**, *4*, 100029. [CrossRef]
3. Shishkin, A.; Bumanis, G.; Irtiseva, K.; Ozolins, J.; Korjakins, A. Clay Ceramic Hollow Sphere—Cement Syntactic Foam Composite for Building Applications. *Key Eng. Mater.* **2019**, *800*, 228–234. [CrossRef]
4. Shishkin, A.; Laksa, A.; Shidlovska, V.; Timermane, Z.; Aguedal, H.; Mironov, V.; Ozolins, J. Illite Clay Ceramic Hollow Sphere-Obtaining and Properties. *Key Eng. Mater.* **2016**, *721*, 316–321. [CrossRef]
5. Khalil, N.; Assaad, J.J. Bond properties between smooth carbon fibre-reinforced polymer bars and ultra-high performance concrete modified with polymesric latexes and fibres. *Eur. J. Environ. Civ. Eng.* **2021**, 1–18. [CrossRef]
6. Kulakov, V.L.; Terrasi, G.P.; Arnautov, A.K.; Portnov, G.G.; Kovalovs, A. Fastening of a High-Strength Composite Rod with a Splitted and Wedged End in a Potted Anchor Finite-Element Analysis. *Mech. Compos. Mater.* **2014**, *50*, 39–50. [CrossRef]

7. Signorini, C.; Volpini, V. Mechanical Performance of Fiber Reinforced Cement Composites Including Fully-Recycled Plastic Fibers. *Fibers* **2021**, *9*, 16. [CrossRef]
8. Kovalovs, A.; Akishin, P.; Chate, A. Detection Prestress Loss in Prestressed Concrete Slab using Modal Analysis. *IOP Conf. Ser. Mater. Sci. Eng.* **2019**, *471*, 102015. [CrossRef]
9. Ramanathan, S.; Benzecry, V.; Suraneni, P.; Nanni, A. Condition assessment of concrete and glass fiber reinforced polymer (GFRP) rebar after 18 years of service life. *Case Stud. Constr. Mater.* **2021**, *14*, e00494. [CrossRef]
10. Kovalovs, A.; Rucevskis, S.; Akishin, P.; Kolupajevs, J. Numerical Investigation on Detection of Prestress Losses in a Prestressed Concrete Slab by Modal Analysis. *IOP Conf. Ser. Mater. Sci. Eng.* **2017**, *251*, 12090. [CrossRef]
11. Šahmenko, G.; Krasnikovs, A.; Lukašenoks, A.; Eiduks, M. Ultra High Performance Concrete Reinforced with Short Steel and Carbon Fibers. *Environ. Technol. Resour. Proc. Int. Sci. Pract. Conf.* **2015**, *1*, 193–199. [CrossRef]
12. Ali, B.; Qureshi, L.A.; Kurda, R. Environmental and economic benefits of steel, glass, and polypropylene fiber reinforced cement composite application in jointed plain concrete pavement. *Compos. Commun.* **2020**, *22*, 100437. [CrossRef]
13. Hussain, I.; Ali, B.; Akhtar, T.; Jameel, M.S.; Raza, S.S. Comparison of mechanical properties of concrete and design thickness of pavement with different types of fiber-reinforcements (steel, glass, and polypropylene). *Case Stud. Constr. Mater.* **2020**, *13*, e00429. [CrossRef]
14. Kononova, O.; Krasnikovs, A.; Harjkova, G.; Lusis, V. Numerical simulation of mechanical properties for composite reinforced by knitted fabric. *Ebook Congr. Mund.* **2014**, *5*, 2925–2932.
15. Elbehiry, A.; Elnawawy, O.; Kassem, M.; Zaher, A.; Mostafa, M. FEM evaluation of reinforced concrete beams by hybrid and banana fiber bars (BFB). *Case Stud. Constr. Mater.* **2021**, *14*, e00479. [CrossRef]
16. Macanovskis, A.; Krasnikovs, A.; Kononova, O.; Lukasenoks, A. Mechanical Behavior of Polymeric Synthetic Fiber in the Concrete. *Proc. Eng.* **2017**, *172*, 673–680. [CrossRef]
17. Lasenko, I.; Grauda, D.; Butkauskas, D.; Sanchaniya, J.V.; Viļuma-Gudmona, A.; Lusis, V. Testing of physical and me-chanical properties of polyacrylonitrile nanofibers reinforced with succinite and silicon oxide nano particles. *Text. Nanofunct. Text.* Unpublished manuscript.
18. Krasnikovs, A.; Kononova, O.; Machanovskis, A.; Zaharevskis, V.; Akishins, P.; Ruchevskis, S. Characterization of mechanical properties by inverse technique for composite reinforced by knitted fabric. Part 2. Experimental evaluation of mechanical properties by frequency eigenvalues method. *J. Vibroeng.* **2012**, *14*, 691–698.
19. Shen, J.; Zhang, Y. Fiber-reinforced Mechanism and Mechanical Performance of Composite Fibers Reinforced Concrete. *J. Wuhan Univ. Technol. Sci. Ed.* **2020**, *35*, 121–130. [CrossRef]
20. Lusis, V.; Krasnikovs, A. Fiberconcrete with Non-Homogeneous Fibers Distribution. *Environ. Technol. Resour. Proc. Int. Sci. Pract. Conf.* **2013**, *2*, 67. [CrossRef]
21. Benaoum, F.; Khelil, F.; Benhamena, A. Numerical analysis of reinforced concrete beams pre cracked reinforced by composite materials. *Frattura ed Integrità Strutturale* **2020**, *14*, 282–296. [CrossRef]
22. Plizzari, G.; Mindess, S. Fiber-reinforced concrete. In *Developments in the Formulation and Reinforcement of Concrete*; Elsevier: Amsterdam, The Netherlands, 2019; pp. 257–287.
23. Ďubek, M.; Makýš, P.; Petro, M.; Ellingerová, H.; Antošová, N. The Development of Controlled Orientation of Fibres in SFRC. *Materials* **2021**, *14*, 4432. [CrossRef]
24. Herrmann, H.; Goidyk, O.; Braunbrück, A. Influence of the Flow of Self-Compacting Steel Fiber Reinforced Concrete on the Fiber Orientations. In *Short Fibre Reinforced Cementitious Composites and Ceramics*; Advanced Structured Materials Book Series; Springer: Cham, Switzerland, 2019; Volume 95, pp. 97–110.
25. Herrmann, H.; Goidyk, O.; Naar, H.; Tuisk, T.; Braunbrück, A. The influence of fibre orientation in self-compacting concrete on 4-point bending strength. *Proc. Estonian Acad. Sci.* **2019**, *68*, 337. [CrossRef]
26. Krasnikovs, A.; Zaharevskis, V.; Kononova, O.; Lusis, V.; Galushchak, A.; Zaleskis, E. Fiber Concrete Properties Control by Fibers Motion Investigation in Fresh Concrete During Casting. In Proceedings of the 8th International DAAAM Baltic Conference, Industrial Engineering, Tallinn, Estonia, 19–21 April 2012; pp. 657–662. Available online: http://innomet.ttu.ee/daaam/proceedings/pdf/krasnikovs.pdf (accessed on 11 November 2021).
27. Bao, C.; Bi, J.; Xu, D.; Guan, J.; Cheng, W.X. Numerical simulation of the distribution and orientation of steel fibres in SCC. *Mag. Concr. Res.* **2020**, *72*, 1102–1111. [CrossRef]
28. Herrmann, H.; Braunbrück, A.; Tuisk, T.; Goidyk, O.; Naar, H. An Initial Report on the Effect of the Fiber Orientation on the Fracture Behavior of Steel Fiber Reinforced Self-Compacting Concrete. *Adv. Struct. Mater.* **2019**, *95*, 33–50. [CrossRef]
29. Lapsa, V.; Krasnikovs, A.; Strauts, K. Process and Device for Manufacturing Fiberconcrete Non-Homogeneous Structural Elements. LV Patent LV14257, 20 April 2011.
30. *State-of-the-Art Report on Fiber Reinforced Concrete*; ACI Committee: Farmington Hills, MI, USA, 2002; Volume 544.
31. Khabaz, A. Analysis of sliding mechanism of straight steel fibers in concrete and determine the effect of friction. *Arch. Civ. Mech. Eng.* **2017**, *17*, 599–608. [CrossRef]
32. Yoo, D.-Y.; Je, J.; Choi, H.-J.; Sukontasukkul, P. Influence of embedment length on the pullout behavior of steel fibers from ultra-high-performance concrete. *Mater. Lett.* **2020**, *276*, 128233. [CrossRef]
33. Khabaz, A. Performance evaluation of corrugated steel fiber in cementitious matrix. *Constr. Build. Mater.* **2016**, *128*, 373–383. [CrossRef]

34. Vu, D.-T.; Toutlemonde, F.; Terrade, B.; Marchand, P.; Bouteille, S. Numerical Modeling of the Steel Fiber Reinforced Concrete Behavior Under Combined Tensile and Shear Loading by a Micromechanical Model Taking into Account Fiber Orientation. In *Fibre Reinforced Concrete: Improvements and Innovations II. BEFIB 2021*; RILEM Bookseries; Springer: Cham, Switzerland, 2022; pp. 443–455.
35. Dehghani, A.; Aslani, F. Effect of 3D, 4D, and 5D hooked-end type and loading rate on the pull-out performance of shape memory alloy fibres embedded in cementitious composites. *Constr. Build. Mater.* **2021**, *273*, 121742. [CrossRef]
36. Abdallah, S.; Rees, D.W.A. Comparisons Between Pull-Out Behaviour of Various Hooked-End Fibres in Normal–High Strength Concretes. *Int. J. Concr. Struct. Mater.* **2019**, *13*, 27. [CrossRef]
37. Sabuncuoglu, B.; Lomov, S.V. Micro-scale numerical study of fiber/matrix debonding in steel fiber composites. *J. Eng. Fibers Fabr.* **2020**, *15*, 1558925020910726. [CrossRef]
38. Deng, F.; Ding, X.; Chi, Y.; Xu, L.; Wang, L. The pull-out behavior of straight and hooked-end steel fiber from hybrid fiber reinforced cementitious composite: Experimental study and analytical modelling. *Compos. Struct.* **2018**, *206*, 693–712. [CrossRef]
39. Ogunbayo, B.; Aigbavboa, C. *Experimental Investigation of Concrete Block Walls Compressive Strength Using a Non-Destructive Test*; Springer Nature: Berlin/Heidelberg, Germany, 2021; pp. 393–397. [CrossRef]
40. Tatarinov, A.; Shishkin, A.; Mironovs, V. Correlation between ultrasound velocity, density and strength in metal-ceramic composites with added hollow spheres. *IOP Conf. Ser. Mater. Sci. Eng.* **2019**, *660*, 12040. [CrossRef]
41. Mironov, V.; Pundiene, I.; Tatarinov, A.; Baroninsh, J. A Study of Metal-Cement Composites with Additives. *Constr. Sci.* **2014**, *16*, 16–20. [CrossRef]
42. Khabaz, A. Experimental and Numerical Investigation of Single Fiber Pull-Out Tests of Steel Macro-Fiber and Glass Micro-Fiber in a Cementitious Matrix. *J. Test. Evaluation* **2022**, *50*, 20200658. [CrossRef]
43. Macanovskis, A.; Lukasenoks, A.; Krasnikovs, A.; Stonys, R.; Lusis, V. Composite Fibers in Concretes with Various Strengths. *ACI Mater. J.* **2018**, *115*, 647–652. [CrossRef]
44. Da Silva, C.N.; Ciambella, J.; Barros, J.; Valente, T.D.S.; Costa, I. A multiscale model for optimizing the flexural capacity of FRC structural elements. *Compos. Part B Eng.* **2020**, *200*, 108325. [CrossRef]
45. Kononova, O.; Lusis, V.; Galushchak, A.; Krasnikovs, A.; Macanovskis, A. Numerical modeling of fiber pull-out mi-cromechanics in concrete matrix composites. *J. Vibroeng.* **2021**, *14*, 1852–1861.
46. Lusis, V. Effect of short fibers orientation on mechanical properties of composite material—Fiber reinforced concrete. *J. Civ. Eng. Manag.* **2017**, *23*, 1091–1099. [CrossRef]
47. Medina, N.F.A.; Lameiras, R.D.M.; Dos Santos, A.C.P.; Willrich, F.L. Effect of Distribution and Orientation of Fibers on the Post-cracking Behavior of Steel Fiber Reinforced Self-compacting Concrete in Small Thickness Elements. In *Fibre Reinforced Concrete: Improvements and Innovations. BEFIB 2020*; RILEM Bookseries; Springer: Cham, Switzerland, 2021; pp. 279–289. [CrossRef]
48. Dvorkin, L.; Zhitkovsky, V.; Ribakov, Y.; Dvorkin, O. A method for optimal design of steel fiber reinforced concrete composition. *Mater. Des.* **2011**, *32*, 3254–3262. [CrossRef]
49. Bleive, L.L.; Lusis, V. Experimental study and numerical modelling for flexural capacity of frc structural elements. *Environ. Technol. Resour. Proc. Int. Sci. Pract. Conf.* **2021**, *3*, 30–35. [CrossRef]
50. Babych, E.; Andriichuk, O.; Ninichuk, M.; Kysliuk, D. Experimental Research of Strength Characteristics of Continuous Reinforced Concrete Beams with Combined Reinforcement, and Modelling Their Work by the Finite Element Method. In *Proceedings of EcoComfort 2020*; Lecture Notes in Civil Engineering; Springer: Cham, Switzerland, 2021; pp. 18–25.
51. Raju, R.A.; Lim, S.; Akiyama, M.; Kageyama, T. Effects of concrete flow on the distribution and orientation of fibers and flexural behavior of steel fiber-reinforced self-compacting concrete beams. *Constr. Build. Mater.* **2020**, *262*, 119963. [CrossRef]
52. Li, L.; Xia, J.; Chin, C.; Jones, S. Fibre Distribution Characterization of Ultra-High Performance Fibre-Reinforced Concrete (UHPFRC) Plates using Magnetic Probes. *Materials* **2020**, *13*, 5064. [CrossRef] [PubMed]